Progress In Electromagnetics Research Letters, Vol. 71, 117–123, 2017

A Dual-Band MIMO Antenna Using a Passive Circuit for Isolation Enhancement

Peng Cheng, Deming Sun, Peng Wang*, and Peng Gao

Abstract—This letter presents a two-port dual-band multiple-input-multiple-output (MIMO) antenna, which is achieved based on a non-radiation passive circuit. The circuit is composed of two pairs of open-ended stubs and a transmission line connecting them. The decoupling condition of $S_{21} = 0$ is deduced, thus a good isolation is achieved. Then this non-radiation circuit is further designed to be a structure with enough radiation without affecting the character of port isolation. Since the implementation of port isolation does not adopt complex decoupling network or decoupling structure, the process of design is simple and effective. The simulation and physical demonstration obtain good agreements for the proposed dual-band MIMO antenna.

1. INTRODUCTION

With the rapid growth in demand for wireless communication technology, multi-band wireless terminals, including the Long Term Evolution (LTE) and wireless local networks (WLAN), are significant for practical devices and have attracted much attention. To obtain high reliability and high data rates, multiple-input-multiple-output (MIMO) technology has been proven to be a good choice due to its unique attributes in terms of enhancing reliability and increasing the channel's capacity. However, the performance of the multi-antenna technology can get significantly bad due to unavoidable mutual couplings among neighboring antennas in practice. Accordingly, keeping high isolation among the antenna elements and ensuring the lowest correlation in a complex scattering environment are very necessary and challenging tasks, and compactness and decoupling are more troublesome in the case that the space reserved for the antenna design is more and more restricted, especially for multi-band antennas.

Over the past few years, a lot of work on developing decoupling techniques has been devoted to reducing the undesired coupling between antennas effectively. The existing decoupling mechanisms can be roughly divided into two categories. The first category employs decoupling structures such as a neutralization line [1, 2], defected ground structure (DGS) [3] and electromagnetic band gap (EBG) [4]. The second type of decoupling techniques applies decoupling networks such as coupled-resonator decoupling network (CRDN) [5], lumped network [6] and LC low-pass π network [7]. In these researches, although these decoupling techniques exhibit good behavior in isolation among the antenna ports, they mostly focus on decoupling between two single band antennas. Their decoupling structure or decoupling network is often complex, and the matching structure is relatively large, which not only increases the difficulty of manufacturing, but also makes it difficult to integrate into the limited space of the practical system. Moreover, the decoupling structures are added after the development of radiation performance, that is to say, achieving port isolation is the final phase of MIMO antenna design.

Received 24 August 2017, Accepted 24 October 2017, Scheduled 20 November 2017
* Corresponding author: Peng Wang (wangpeng@uestc.edu.cn).
The authors are with the Research Institute of Electronic Science and Technology, Information Geoscience Research Center, University of Electronic Science and Technology of China, Chengdu, China.

Recently, a new approach is proposed for developing MIMO antenna in [8]. Compared with conventional decoupling techniques, the decoupling approach based on a non-radiation circuit model is different and innovative in that the isolation obtained through two signal paths canceled out mutually before achieving ideal radiating performance. This method utilizes the isolation nature of certain passive networks to derive antennas with decoupling ensured in the first place, rather than introducing decoupling structures at the last stage of MIMO antenna design. However, the antenna could only operate at single frequency band; meanwhile, the mono-radiator antenna has a large dimension. In this paper, this method is further exploited to design a dual-band MIMO antenna.

2. ANTENNA DESIGN AND ANALYSIS

2.1. The Decoupling Analysis of Antenna

In this paper, isolation is the first issue to discuss. To design a dual-band MIMO antenna with good port isolation, primarily, a passive circuit model with no radiation performance needs to be established to meet the decoupling condition $S_{21} = 0$. Afterwards, a radiative structure is built based on the circuit model. Finally, the antenna is further optimized to achieve high radiation efficiency while maintaining port isolation.

As shown in Figure 1(a), for ensuring dual-band isolation, we propose a circuit composed of a transmission line in connecting two pairs of open-ended stubs, with two feeding ports in both intersections. Their characteristic impedances and electrical lengths are named (Z_1, θ_1), (Z_2, θ_2) and (Z_3, θ_3), respectively. For the above two-port network, to investigate the transmission characteristics, the ABCD matrices of stub1, stub2 and line in Figure 1(b) are given, respectively, as

$$M_{\text{stub1}}=\begin{bmatrix} 1 & 0 \\ jY\tan\theta_1 & 1 \end{bmatrix}, \quad M_{\text{stub2}}=\begin{bmatrix} 1 & 0 \\ jY\tan\theta_2 & 1 \end{bmatrix}, \quad M_{\text{line}}=\begin{bmatrix} \cos\theta_3 & jY_3\sin\theta_3 \\ jY_3\sin\theta_3 & \cos\theta_3 \end{bmatrix}$$

So, the whole circuit $ABCD$ matrices M can be obtained according to the following formula:

$$M = (M_{\text{stub1}} \| M_{\text{stub2}}) * (M_{\text{line}}) * (M_{\text{stub1}} \| M_{\text{stub2}}) \tag{1}$$

Further, after S-parameter conversions, the S_{21} can be derived as follows:

$$S_{21}=\frac{2}{A + B/Z_0 + CZ_0 + D} \tag{2}$$

Here Z_0 represents the input port impedance. Thus, we can enforce and simplify the isolation condition of $S_{21} = 0$, which can be ultimately expressed as Eq. (3):

$$\cot\theta_1 \cot\theta_2 = 0 \tag{3}$$

Obviously, Eq. (4) is the solutions of Equation (3).

$$\theta_1 = \pi/2 + n\pi \cdot \text{ or } \cdot \theta_2 = \pi/2 + n\pi \tag{4}$$

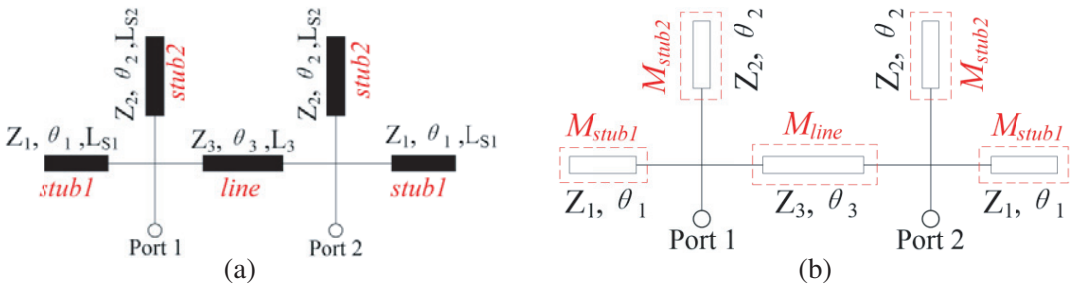

Figure 1. (a) Equivalent circuit model. (b) The corresponding two-port network.

From Eq. (4), it is easily seen that there are many solutions to these electrical lengths, and the electric lengths L_{S1} and L_{S2} are quarter wavelengths corresponding to the frequencies of f_{S1} and f_{S2}. In contrast, frequencies can be determined by Eq. (5).

$$f_{S1}=\frac{c}{4L_{s1}\sqrt{\varepsilon}_{\text{eff}}}, \quad f_{S2}=\frac{c}{4L_{s2}\sqrt{\varepsilon}_{\text{eff}}} \tag{5}$$

where c stands for the speed of light in free space, and ε_{eff} is the effective dielectric constant of the medium. Eq. (5) reveals that the two frequencies are determined by the length parameters L_{S1} and L_{S2}, respectively. To verify the above results, simulation is carried out in ADS. Figure 2 describes the S_{21} characteristics with different L_{S2} and L_{S1}. Obviously, two transmission zeros are generated, which is consistent with expectation. Figure 2(a) shows that when L_{S2} varies from 22.6 to 25.8 mm, the transmission zero of the lower frequency decreases from 2.4 to 2.1 GHz; meanwhile, the transmission zero remains unchanged at higher frequency. Similarly, the transmission zero of the higher frequency can be adjusted by changing L_{S1}, and it has no influence on the transmission zero of the low frequency, as shown in Figure 2(b). In other words, varying one stub length only affects one transmission zero while the other zero is fixed by the other stub length, and shorter stub length of L_{S1} and longer sub length of L_{S2} determine the upper and lower zeros, respectively. Hence, good validation is obtained for the above analysis.

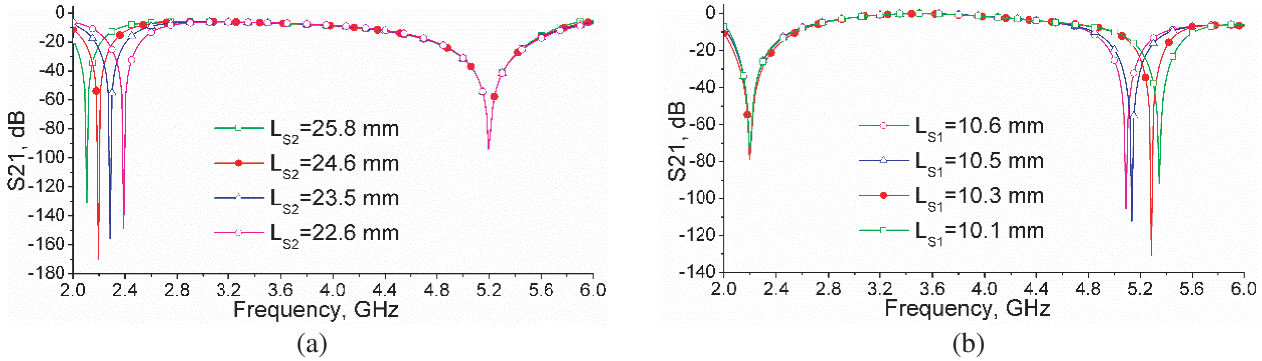

Figure 2. Simulated S_{21} of the equivalent circuit model with different dimension. (a) L_{S2} and (b) L_{S1}.

2.2. The General Idea and Method of the Designed Antenna

As can be observed from Formula (4), the smallest size of circuit can be achieved choosing θ_1 and θ_2 both at their minimum value of $\pi/2$, when $n = 0$. Therefore, we can basically build a microstrip structure with radiating ability from this circuit model, including two pairs of open-ended strips and a strip in the middle. The impedances and electrical lengths of the strips should meet the isolation condition in Eq. (3). When good port isolation is guaranteed in two frequency bands, further use HFSS to optimize each parameter for making the antenna achieve high radiation efficiency while maintaining port isolation. To verify the above design analysis and feasibility of the circuit model, the detailed design process and realization are illustrated by the following example.

2.3. The Design Process of Antenna

Based on the above analysis, according to Eq. (4), when a simple case $n = 0$, the electrical lengths θ_1 and θ_2 both are $\pi/2$. Thus, a structure of the proposed dual-band MIMO antenna designed on a 1.6 mm thick FR4 substrate with relative permittivity of 4.4 and loss tangent of 0.02 is shown in Figure 3(a). The center frequency f_{S2} of the lower band is chosen as 2.20 GHz, and the effective quarter wavelength is estimated at around 22 mm between 34 mm in air and 25 mm in FR4. Therefore, L_{S2} ($L_{S2} = L4+L5$) is about 22 mm. The center frequency f_{S1} of the higher band is selected to be 5.25 GHz, and the effective quarter wavelength is set at around 10 mm because the quarter wavelength of 5.25 GHz is 14 mm in air and 10.4 mm in FR4, hence, the length of the open-ended strip L_{S1} ($L_{S1} = L3$) is initially estimated

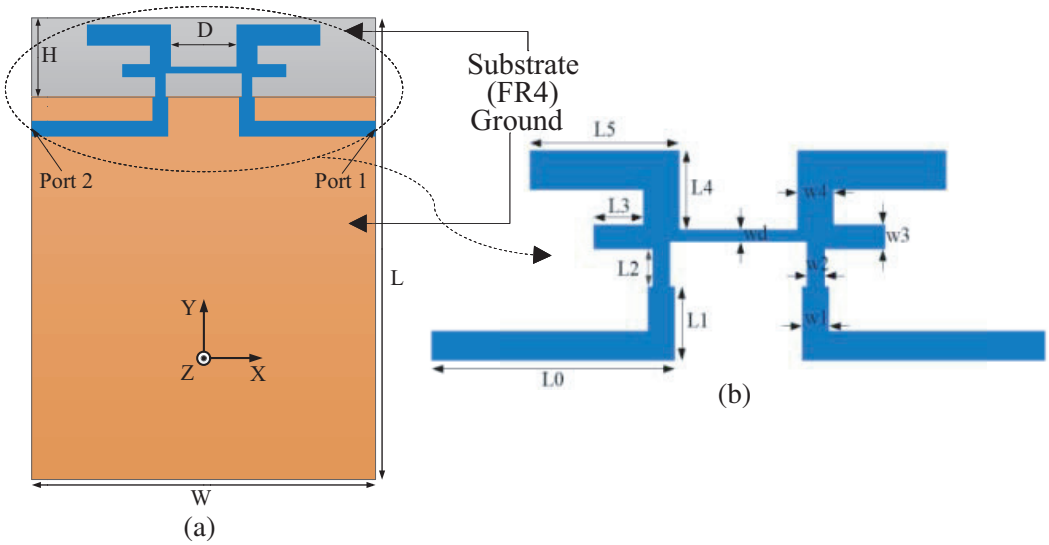

Figure 3. Dimensions of the MIMO antennas. (a) General view and (b) dimensions of the antenna.

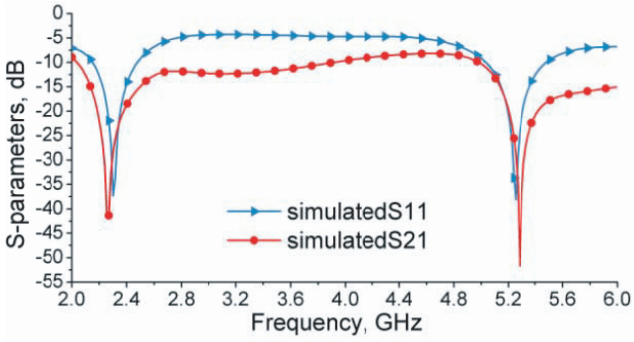

Figure 4. The simulated S-parameters of the proposed antenna.

Table 1. Structural parameters of the proposed antenna. (mm).

Variable	Value	Variable	Value	Variable	Value	Variable	Value	Variable	Value
W	63	$L1$	6.3	$w1$	2.3	$w4$	4	$L2$	4.3
L	77.6	D	11.5	$w2$	1.5	$L3$	5	$L5$	17
H	17.6	$L0$	25	$w3$	2.5	$L4$	9.3	wd	1.4

to be 10 mm. After optimization, the final simulated results are shown in Figure 4, which shows that the return losses S_{11} are all below -10 dB within the two operating bands of 2.10–2.49 GHz and 5.10–5.42 GHz. At the same time, the excellent performance of port isolation is maintained. Desirable S-parameter performances of the presented dual-band antenna are achieved. The final antenna structure is shown in Figure 3, and the optimized structural parameters are concluded in Table 1.

3. EXPERIMENTAL RESULTS AND DISCUSSION

The designed antenna is manufactured and measured. Its photographs of top and back views are shown in Figure 5. Figure 6 illustrates that the measured S-parameters agree well with simulation results. As shown in Figure 6, the measured -10 dB impedance bandwidth of the lower band is from 2.10 to

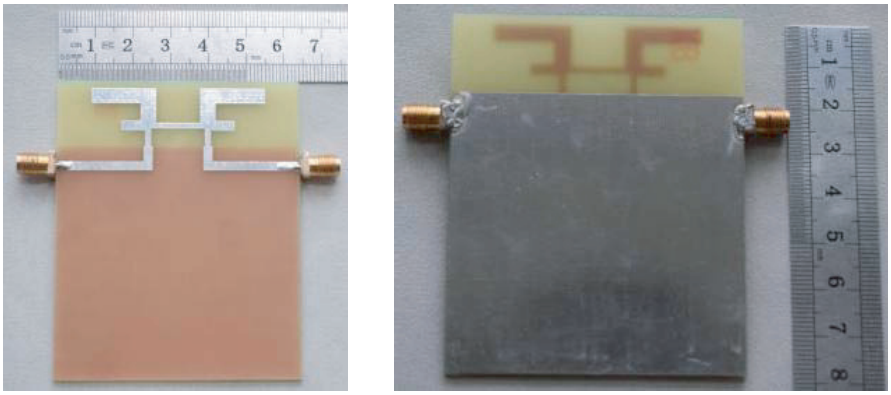

(a) (b)

Figure 5. Photographs for fabricated antenna sample. (a) Top view. (b) Back view.

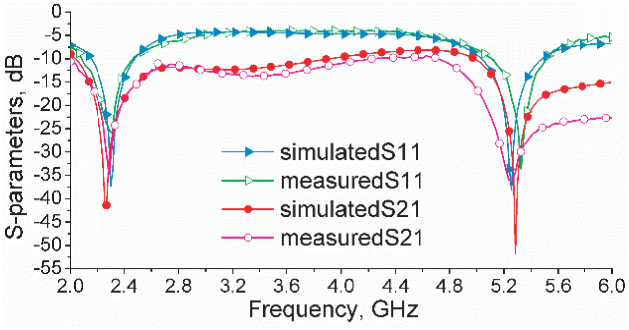

Figure 6. Measured and simulated S-parameter results of the proposed antenna.

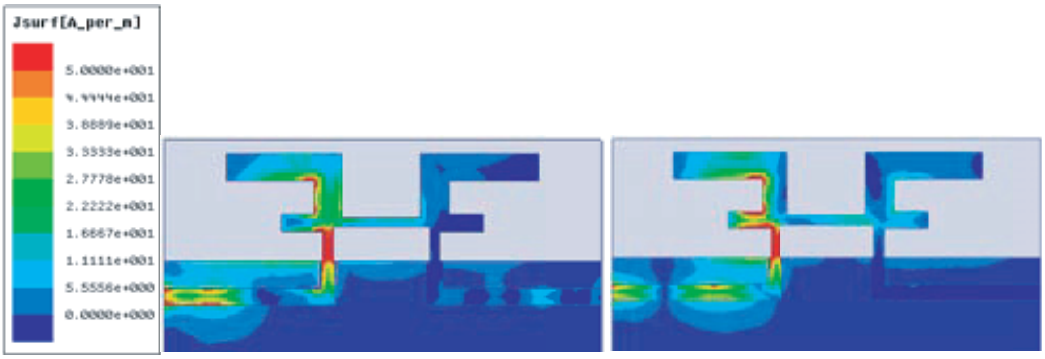

(a) (b)

Figure 7. Simulated current distributions. (a) 2.2 GHz. (b) 5.25 GHz.

2.49 GHz, and the upper band is from 5.10 to 5.42 GHz. It is noted that the port isolation is better than 15 dB in both the operating bands. Figure 7 shows the surface current distributions of the MIMO antenna, and it can be observed that the left excited port is isolated from the right port at the center frequencies of 2.2 and 5.25 GHz, respectively.

Figure 8 presents the simulated and measured radiation patterns at 2.20 and 5.25 GHz, respectively. When port 1 is excited, port 2 is connected by a matched load. It is shown that the simulated results are in good agreement with the measured ones. The XZ-plane and YZ-plane are omnidirectional in the two operating bands, and the radiation patterns of XY, XZ and YZ planes have good complementarity.

Diversity performance is analyzed to characterize the MIMO antenna system, and the diversity

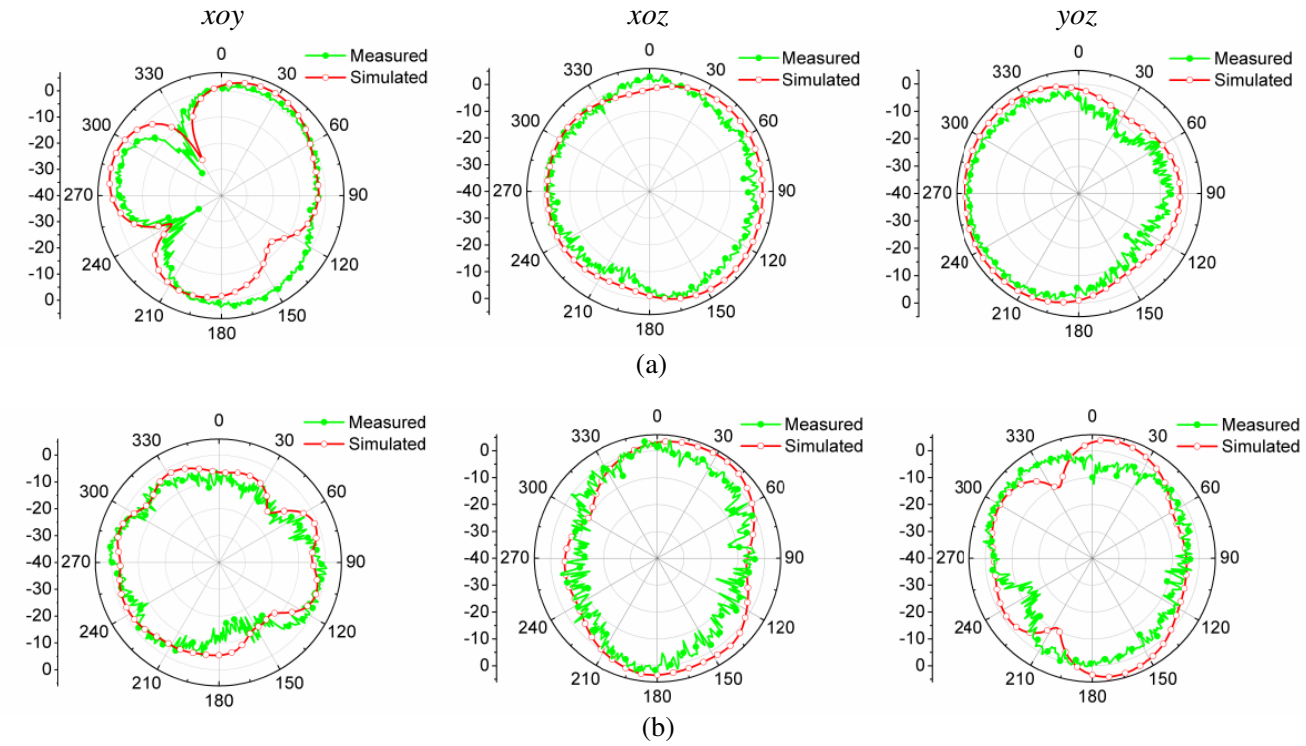

Figure 8. Radiation patterns of the proposed MIMO antenna. (a) 2.2 GHz. (b) 5.25 GHz.

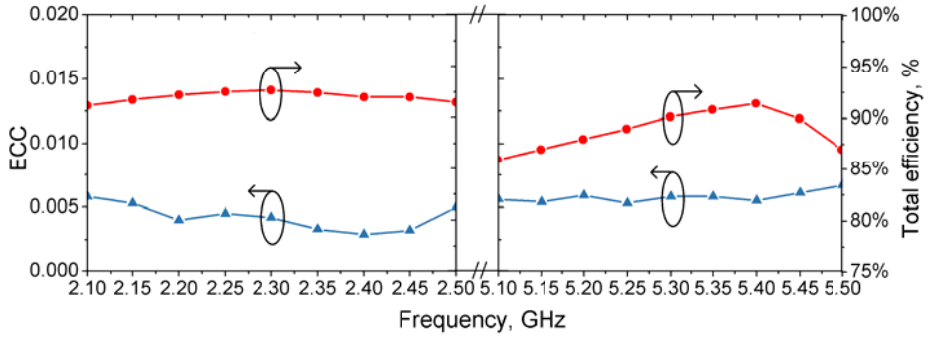

Figure 9. Calculated ECC and simulated total efficiency of the proposed antenna.

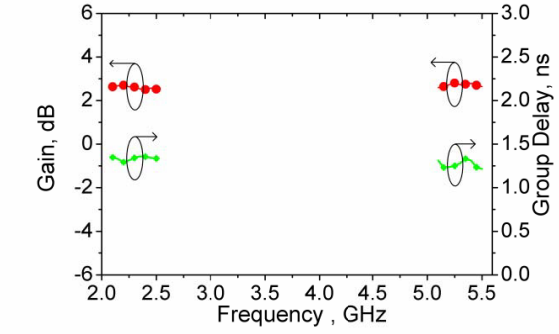

Figure 10. Measured total gain and group delay for the proposed antenna.

performance of the proposed MIMO antenna can be evaluated from its envelope correlation coefficient (ECC). The formula to express ECC is given in [9]. As shown in Figure 9, the ECC of the proposed antenna is below 0.01 within the two operating bands, which indicates that a great diversity performance of the MIMO antenna can be realized. Figure 9 also shows that the simulated total efficiency is above 85% in the two operating bands. The measured results of peak gain and group delay are shown in Figure 10. The average peak gains are approximately 2.56 dBi in the lower band 2.1–2.49 GHz and 2.67 dBi in the higher band 5.10–5.49 GHz, respectively. It can be illustrated that the presented antenna demonstrates available and stable gain in the two operating bands. The measured group delay of the proposed antenna is almost constant. This confirms that the proposed antenna is suitable for communications.

4. CONCLUSION

A novel structure of a dual-band MIMO antenna is designed, fabricated and investigated in this Letter. Since no complex decoupling and matching networks are introduced, the proposed dual-band MIMO antenna is very simple and compact. So it is a good choice for miniaturization without increasing the footprint. The two bands cover 2.10–2.49 GHz and 5.10–5.42 GHz, and the experimental result demonstrates that the proposed MIMO antenna is very suitable for UMTS 2100, LTE 2300 and 2.4 GHz WLAN band applications due to the good performances in S-parameters, radiation patterns and ECC. In addition, compared to the present decoupling technologies for the dual-band antenna, the new approach proposed in this paper of deriving MIMO antenna from port-isolated non-radiative passive circuit can also be used as an effective solution for developing MIMO antennas. The proposed method will be further studied in the future work.

REFERENCES

1. Su, S. W., C. T. Lee, and F. S. Chang, "Printed MIMO-antenna systems using neutralization-line technique for wireless USB-dongle applications," *IEEE Antennas and Wireless Propagation Letters*, Vol. 60, No. 2, 456–463, 2012.
2. Khan, M. S., M. F. Shafique, A. Naqvi, A. D. Capobianco, B. Ijaz, and B. D. Braaten, "A miniaturized dual-band diversity antenna for WLAN applications," *IEEE Antennas and Wireless Propagation Letters*, Vol. 14, 958–961, 2015.
3. Li, J. F., Q. X. Chu, and T. G. Huang, "A compact wideband MIMO antenna with two novel bent slits," *IEEE Antennasand Wireless Propagation Letters*, vol. 60, No. 2, 482–489, 2012.
4. Payandehjoo, K. and R. Abhari, "Employing EBG structures in multi-antenna systems for improving isolation and diversity gain," *IEEE Antennas and Wireless Propagation Letters*, Vol. 8, 1162–1165, 2009.
5. Zhao, L. Y., L. K. Yeung, and K. L. Wu, "A coupled resonator decoupling network for two-element compact antenna arrays in mobile terminals," *IEEE Transactions on Antennas and Propagation*, Vol. 62, No. 5, 2767–2776, 2014.
6. Li, R. P., P. Wang, Q. Zheng, and R. Z. Wu, "Compact microstrip decoupling and matching network for two symmetric antennas," *Electronics Letters*, Vol. 51, No. 18, 1396–1398, 2015.
7. Meng, H. and K. L. Wu, "An LC decoupling network for two antennas working at low frequencies," *IEEE Transactions on Antennas and Propagation*, Vol. 65, No. 7, 2321–2329, 2017.
8. Zhang, Y. L. and P. Wang, "Single ring two-port MIMO antenna for LTE applications," *Electronics Letters*, Vol. 52, No. 12, 998–1000, 2016.
9. Vaughan, R. G. and J. B. Andersen, "Antenna diversity in mobile communications," *IEEE Transactions on Vehicular Technology*, Vol. 36, No. 4, 149–172, 1987.